Structural Insights into Enzyme Regulation for Inositol 1,4,5-Trisphosphate 3-Kinase B

Philip P. Chamberlain, Mark L. Sandberg, Karsten Sauer, Michael P. Cooke, Scott A. Lesley, and Glen Spraggon*

Genomics Institute of the Novartis Research Foundation, 10675 John Jay Hopkins Drive, San Diego, California 92121

Received June 30, 2005; Revised Manuscript Received August 18, 2005

ABSTRACT: D-Myoinositol 1,4,5-trisphophate 3-kinases (IP_3-3Ks) play important roles in metazoan cellular signaling. It has been demonstrated that mice without a functional version of IP_3-3K isoform B are deficient in peripheral T-cells, indicating that IP_3-3KB is essential to the developing immune system. The recent apo IP_3-3KA structure exhibited a helix at the catalytic domain N-terminus exhibited a helix at the N-terminus of the catalytic domain, with a tryptophan indole moiety mimicking the binding mode of the substrate ATP purine ring, suggesting a mechanism of autoinhibition. Here we present the structure of the complete catalytic domain of IP_3-3KB, including the CaM binding domain in complex with Mg^{2+} and ATP. The crystal structure reveals a homodimeric arrangement of IP_3-3KB catalytic domains, mediated via an intermolecular antiparallel β-sheet formed from part of the CaM binding region. Residues from the putative autoinhibitory helix are rearranged into a loop configuration, with extensive interactions with the bound ATP. Mutagenesis of residues from this region reveals that substitution of the putative autoinhibitory tryptophan generates a hyperactive enzyme which retains Ca^{2+}/CaM sensitivity. The IP_3-3KB structure suggests a mechanism of enzyme activation, and raises the possibility that an interaction between IP_3-3KB molecules may occur as part of the catalytic or regulatory cycle.

The second messenger D-myoinositol 1,4,5-trisphosphate (IP_3)[1] is generated from phosphatidylinositol 4,5-bisphosphate at the plasma membrane through the action of phospholipase C. IP_3 has been demonstrated to bind to numerous cellular receptors and can mobilize Ca^{2+} in numerous cell types (*1*). IP_3 has a short half-life in the cytoplasm, consistent with an important role in signaling. Removal of IP_3 from the cytoplasmic pool is performed either through the action of 5′-phosphatases or by addition of a 3′-phosphate by an inositol 1,4,5-trisphosphate 3-kinase (IP_3-3K). IP_3-3Ks have been implicated in numerous cellular signaling events in metazoans. These enzymes catalyze the transfer of the γ-phosphate from ATP to the 3′-position of IP_3 to form inositol 1,3,4,5-tetrakisphosphate (IP_4). IP_4 has also been shown to have a short lifetime in the cytoplasm, and can mediate various effects, including Ca^{2+} mobilization, higher-order inositol polyphosphate production, nuclear processes (*1*, *2*), and Erk activation (*3*, *4*). The recent realization that the PH domains of some RasGAPs can bind IP_4 opens avenues toward a mechanistic understanding of IP_4 function (*5*). Thus, as key regulators of IP_3 and IP_4, IP_3-3Ks play a pivotal role in intracellular signaling (*6*).

Three distinct genes encode IP_3-3Ks in mammals, genes A, B, and C which have highly similar catalytic domains but highly variable N-terminal regions (*7*−*9*). The three IP_3-3K isoforms vary in biological function, tissue distribution, and subcellular localization. IP_3-3KA is expressed exclusively in the brain and testis, and has been implicated in long-term potentiation (*10*, *11*). IP_3-3KC has a more general tissue distribution, and the enzyme kinetics of this isoform are consistent with a proposed role in basal IP_3 homeostasis (*12*). IP_3-3KB is expressed in the brain, heart, lung, testis, and thymus (*13*), and has been localized to the plasma membrane, the cytosol, the cytoskeleton, and the cytosolic face of the ER (*14*, *15*).

Mice deficient for each of the IP_3-3K genes have recently been generated and point to a unique role for IP_3-3KB in guiding the development of T-lymphocytes. IP_3-3KB has been shown to be essential for T-cell development in mice, and a complete block in T-cell progression past the $CD4^+$-$CD8^+$ double-positive stage is observed in IP_3-3KB deficient animals (*3*, *16*). Surprisingly, Ca^{2+} levels were not affected in the knockout animals; however, activation of the Ras effector Raf and its downstream target extracellular signal-regulated kinase (Erk) in response to weak antigen stimulation were attenuated (*3*, *4*).

Full-length human IP_3-3KB is a protein of 946 residues; the mouse and rat proteins are 942 and 934 residues in length, respectively (*17*). The nascent protein is composed of an N-terminal region containing a membrane anchoring region (*18*), a putative PEST sequence (discussed below), and a CaM binding domain immediately N-terminal to the catalytic domain which exists at the C-terminus (*6*). The level of sequence identity of the CaM binding and catalytic domains

* To whom correspondence should be addressed. Phone: (858) 812-1567. Fax: (858) 812-1746. E-mail: gspraggon@gnf.org.

[1] Abbreviations: MPD, methylpentanediol; PEG, polyethylene glycol; ASU, asymmetric unit; CCD, charge-coupled device; NCS, noncrystallographic symmetry; TCEP, tris(2-carboxyethyl)phosphine hydrochloride; DTT, dithiothreitol; IP_3, D-myoinositol 1,4,5-trisphosphate; IP_4, D-myoinositol 1,3,4,5-tetrakisphosphate; HEPES, 4-(2-hydroxyethyl)-1-piperazineethanesulfonic acid; AID, autoinhibitory domain; PKA, cyclic AMP-dependent protein kinase; rmsd, root-mean-square deviation.

10.1021/bi051256q CCC: $30.25
Published on Web 10/14/2005

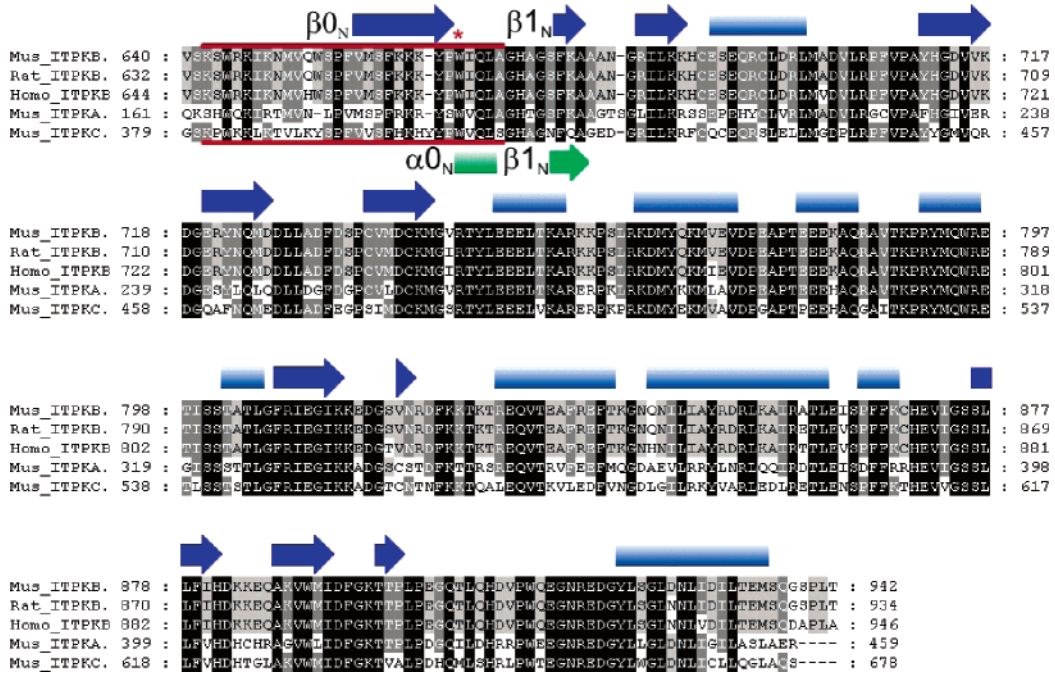

FIGURE 1: Sequence alignment of IP_3-3Ks. The CaM binding domain is indicated in red. IP_3-3KB secondary structure is indicated in blue above the sequence alignment, and IP_3-3KA secondary structure elements $\alpha 0_N$ and $\beta 1_N$ are indicated in green below the corresponding sequence. Trp186 and Trp666 (IP_3-3KA and IP_3-3KB, respectively) are indicated with a red asterisk.

among the three IP_3-3K isoforms is ~65%. For simplicity, residue numbering in this paper has been normalized to the mouse IP_3-3K sequences (Figure 1).

IP_3-3K enzymatic activity is regulated through numerous mechanisms. Recombinant, purified IP_3-3K activity is enhanced by Ca^{2+}/CaM in a manner that does not affect the K_m for IP_3 (*19*). IP_3-3KB has a lower basal enzyme activity than IP_3-3KA, but is stimulated to a greater degree by the presence of Ca^{2+}/CaM, with 2.5- and 20-fold increases in activity for IP_3-3KA and IP_3-3KB, respectively. The site of the CaM binding domain has been shown by deletion mapping to reside between IP_3-3KA residues 163 and 190 (Figure 1) (*20*, *21*). Trp165 or Trp644 (IP_3-3KA or IP_3-3KB, respectively) is conserved across the IP_3-3Ks, and mutation of this residue abolishes Ca^{2+}/CaM activation by IP_3-3KA without destroying enzymatic activity (*21*).

Phosphorylation of IP_3-3Ks has been demonstrated by PKA, PKC, and CaM-dependent protein kinase II (CaMKII) (*22*, *23*). CaMKII has been shown to phosphorylate IP_3-3KA residue Thr311, resulting in an up to 10-fold activation, and a 25-fold increase in sensitivity to Ca^{2+}/CaM (*23*). PKA phosphorylation of IP_3-3KA results in an ~2-fold increase in V_{max}, while PKC phosphorylation gives an ~4-fold reduction in activity compared to that of the unphosphorylated enzyme (*19*, *22*). Phosphorylation of IP_3-3KA by PKA and PKC induces similar fold differences in enzyme activity in the presence or absence of Ca^{2+}/CaM. In contrast, basal IP_3-3KB activity is unaffected by phosphorylation by PKA or PKC, and it is only in the presence of Ca^{2+}/CaM that a 45 or 70% reduction in activity compared to that of the unphosphorylated enzyme is observed for PKA or PKC phosphorylation, respectively.

Proteolysis also plays an important role in IP_3-3K regulation, and IP_3-3KB has been shown to be a substrate for calpain at several sites N-terminal of the catalytic domain, with in vitro proteolysis ultimately yielding a 35 kDa fragment which retains enzymatic activity. Furthermore, calpain cleavage has been demonstrated to liberate IP_3-3KB from the membrane (*18*). Several CaM-regulated proteins are regulated by proteolysis, and cleavage has been shown to occur at PEST sequences (*24*). In studied instances of PEST-containing proteins, cleavage by calpain has been demonstrated to occur at positions other than the PEST regions, and often within the CaM binding region (*25*). This is consistent with the observation that Ca^{2+}/CaM binding protects against the calpain cleavage which generates the 35 kDa catalytic fragment (*18*). Since it has been demonstrated that only N-terminal truncations result in an active enzyme (*20*), the 35 kDa ITPKB fragment is expected to be the most C-terminal region.

Although the sequences of IP_3-3Ks are not significantly similar to those of other kinase classes, recent structures of IP_3-3KA revealed that these proteins share a common topology and active site architecture with the protein kinases (*26*, *27*). In the apo IP_3-3KA structure, the $\alpha 0_N$ helix occupies the ATP binding site with the indole moiety of conserved IP_3-3KA residue Trp186 mimicking the position and some of the interactions formed by the ATP purine ring. By competing with the ATP substrate in this conformation and stabilizing the apo form of the enzyme, IP_3-3KA exhibited a mechanism of autoinhibition (*26*). Pseudosubstrate autoinhibition is a common mechanism of enzyme regulation and has been well documented for protein kinases (*28*). However, a reduction in activity to 44% of the WT value was reported for the W186A IP_3-3KA mutant (*26*). Unfortunately, residue 186 was disordered in the IP_3-3KA holo structures, and no explanation could be offered to rationalize the molecular and structural data.

Here we present the structure of the complete catalytic domain and part of the N-terminal CaM binding domain of IP_3-3KB, in complex with ATP and Mg^{2+}. The predicted molecular mass for this fragment is 35 004 Da, and it is

therefore likely to be close in sequence to the 35 kDa catalytic fragment generated by calpain proteolysis. The IP_3-3KB structure completes the definition of the IP_3-3K catalytic domain by including active site residues disordered in the published holo IP_3-3KA structures. Newly defined regions include residues from the putative autoinhibitory sequence containing Trp666 (equivalent to IP_3-3KA Trp186), which is in fact revealed to play a role in ATP binding. The structure of the CaM binding domain offers a structural explanation for IP_3-3KB regulation by Ca^{2+}/CaM, by linking residues in the CaM binding domain to residues contacting ATP bound in the enzyme active site. Finally, the IP_3-3KB structure reveals a homodimeric arrangement of catalytic domains, linked by an antiparallel β-sheet formed by residues in the CaM binding domain.

EXPERIMENTAL PROCEDURES

The DNA sequence encoding murine IP_3-3KB residues 640−942 was amplified from a full-length construct in mammalian expression vector pKDNZ by PCR. The 3′-primer incorporated a stop codon and an overhanging PacI site. The product was digested with PacI before being ligated into the MH4 plasmid which had been prepared by digestion with PmlI and PacI. Cloning into the MH4 plasmid added the sequence MGSDKIHHHHHH to the N-terminus of the translated region. Mutant enzymes were made by site-directed mutagenesis using the Stratagene Quikchange kit.

IP_3-3KB was expressed in the HK100 strain of *Escherichia coli*. Typically, 4 L of cells was grown in LB with 0.1 μg/mL ampicillin to 0.5A_{600} at 30 °C, before induction with 0.02% L-arabinose for 6 h. Cells were harvested by centrifugation, and pellets were resuspended in 50 mL of 50 mM Tris (pH 8), 100 mM NaCl, 1 mM TCEP, and 0.1 mg/mL lysozyme, with 1 Complete protease inhibitor tablet (Roche). Cells were disrupted by sonication, and debris was removed by centrifugation for 40 min at 35000*g*.

Initial purification was performed using three nickel−Sepharose Hi-Trap HP 1 mL columns (Amersham) connected in series. After application of the pellet supernatants, the bound material was washed with 20 mM Tris (pH 8.0), 20 mM imidazole, 10% glycerol (v/v), and 1 mM TCEP before elution with an imidazole gradient up to 200 mM. IP_3-3KB intended for kinetic experiments was concentrated and frozen as described below at this time. The nickel column eluate for crystallization was diluted 5-fold into 20 mM Tris (pH 8), 10% glycerol, and 1 mM DTT and loaded onto a 6 mL ReSource Q anion exchange chromatography column (Amersham), with elution by a NaCl gradient to 100 mM.

Fractions containing IP_3-3KB were identified by SDS−PAGE, and the pure fractions were concentrated and buffer exchanged using centriprep 20 15 kDa columns into 20 mM Tris (pH 8), 200 mM KCl, 5 mM $MgCl_2$, 0.5 mM DTT, 10% glycerol, 1 μM IP_3, and 20 μM ATP to a final protein concentration of 7 mg/mL.

IP_3-3KB activity was determined using the Kinase-Glo (Promega) ATP depletion assay. The assay reaction buffer consisted of 50 mM Tris (pH 8.0), 100 mM NaCl, 1 mM DTT, 10% glycerol, 5 mM $MgCl_2$, and 1 μM ATP. Each 40 μL reaction mixture contained the indicated concentrations of IP_3 (Alexis Biochemicals), calmodulin (Biomol), $CaCl_2$, and EGTA. Upon addition of purified IP_3-3KB (final concentration of 120 nM), the reaction mixture was incubated for 15 min at room temperature and the reaction subsequently stopped by the addition of an equal volume of kinase-glo reagent. Luminescence was measured using a Molecular Devices Acquest instrument. Data points and error bars shown in Figure 2 are the result of three experiments.

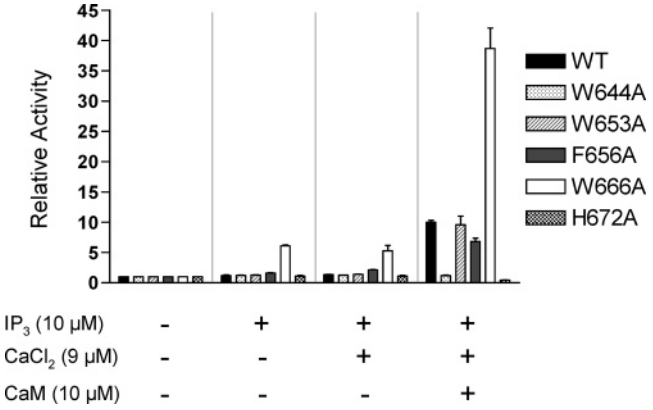

FIGURE 2: ATPase activity compared to the no IP_3 control showing Ca^{2+}/CaM responsiveness of WT and mutant IP_3-3KB constructs.

Table 1: Crystallographic Statistics for IP_3-3KB

data collection site	ALS 5.0.2
wavelength (Å)	1.00
space group	*P*1
resolution range (Å)	50−2.5 (2.59−2.5)[a]
cell dimensions (Å)	$a = 53.2$, $b = 60.7$, $c = 56.9$
angles (deg)	$\alpha = 59.9$, $\beta = 72.7$, $\gamma = 88.2$
no. of observations	52221
no. of unique reflections	19362 (1697)[a]
completeness (%)	95.3 (83.1)[a]
$I/\sigma I$	16.8 (3.0)[a]
R_{merge}[b]	0.081 (0.30)[a]
refinement statistics	
rmsd for bond lengths (Å) and angles (deg)	0.014/1.70
R_{work}/R_{free}[c]	18.5/27.0
mean *B* factor (protein/ligand)	36.4/19.2
rmsd for *B* factor (main chain bond/side chain bond)	0.72/1.81

[a] Figures in parentheses are for the outer resolution shell.

[b] $R_{merge} = \sum_{hkl}\sum_{j}|I_j(hkl) - \langle I(hkl)\rangle| / \sum_{hkl}\sum_{j}|I_j(hkl)|$.

[c] $R = \sum_{h,k,l}|F_{obs}(h,k,l) - F_{calc}(h,k,l)| / \sum_{h,k,l}|F_{obs}(h,k,l)|$

Crystallization was by the sitting drop method. Crystals formed when the protein solution was mixed 1:1 with and subsequently equilibrated against a reservoir solution of 100 mM HEPES (pH 7.0) and 20% PEG3350 for 4 days at 4 °C. Crystals were cryoprotected by being transferred into a solution containing 18% PEG3350, 100 mM HEPES (pH 7.0), 100 mM KCl, 5 mM $MgCl_2$, 10% ethylene glycol, and 10% MPD, before being flash-frozen in liquid nitrogen. Diffraction initially only extended to ~3 Å in space group *C*2. However, by elevating the PEG3350 levels to 25−30% in the cryoprotection buffer and soaking the crystals for 2 min, we improved the diffraction quality to 2.5 Å, although a distortion in the crystal lattice caused a change in space group to *P*1.

Data were collected at the Advanced Light Source (ALS) (Berkeley, CA) beamline 5.0.2. The data set summarized in

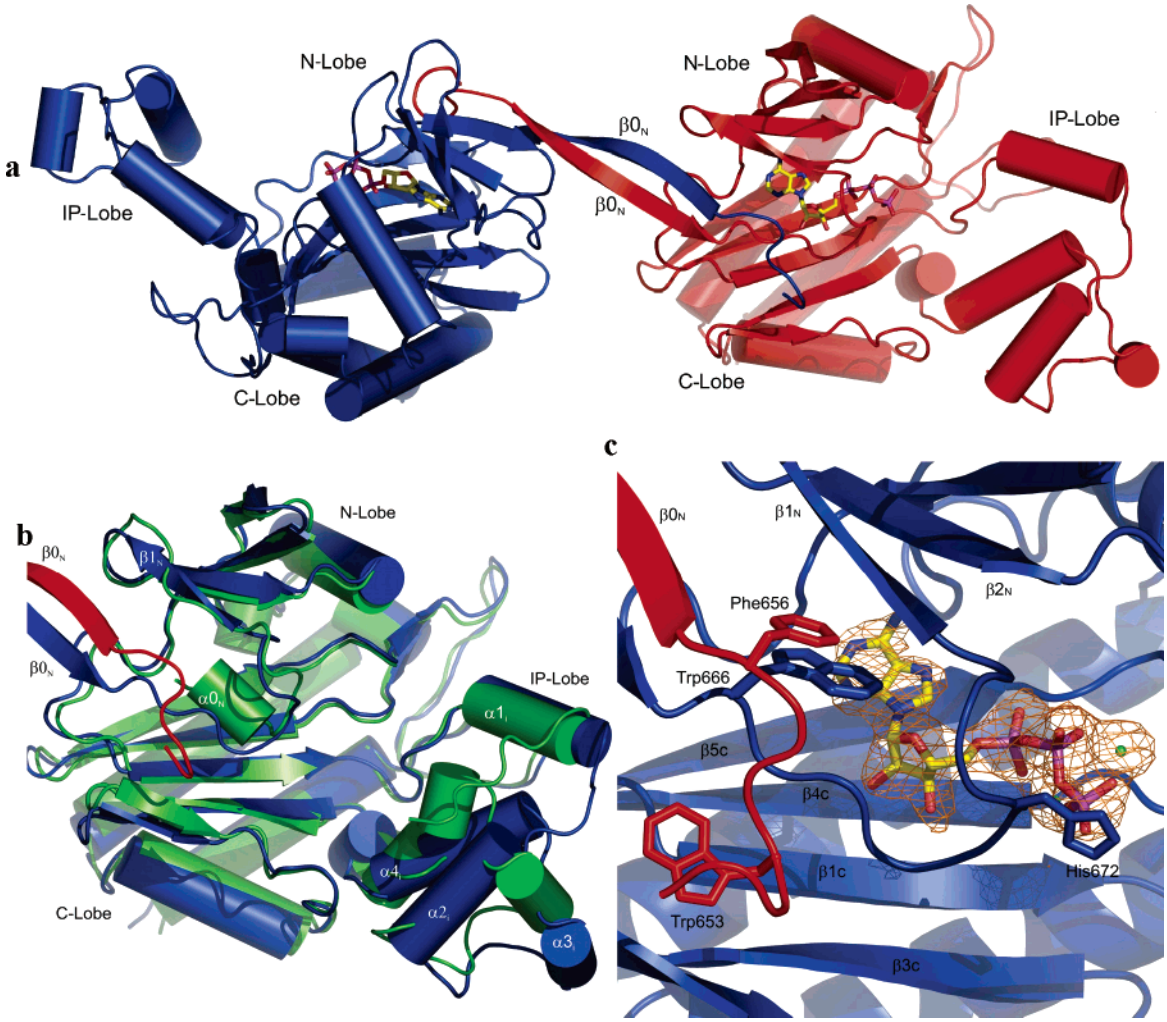

FIGURE 3: (a) Two IP_3-3KB catalytic domains, colored blue (chain A) and red (chain B), linked by an antiparallel β-sheet ($\beta 0_N$) formed by part of the CaM binding domain. (b) Structural alignment of IP_3-3KB with apo IP_3-3KA. IP_3-3KB chains A and B are colored blue and red, respectively; apo IP_3-3KA is colored green. Secondary structure elements $\beta 0_N$ (IP_3-3KB only) and $\alpha 0_N$ (IP_3-3KA only) are labeled. (c) ATP bound in the active site of IP_3-3KB showing omit difference density for the ATP contoured at 3σ. The coloring scheme is the same as for panel a, with Mg^{2+} ions depicted as green spheres. Side chains are shown for residues mutated for Figure 2 with the exception of residue 644, which was disordered in the structure.

Table 1 was collected at 100 K using a 3 × 3 CCD. Data were integrated, reduced, and scaled using HKL2000 (*29*) and the CCP4i suite (*30*). Crystallographic statistics are summarized in Table 1. The IP_3-3KB structure was determined by molecular replacement using Phaser (*31*) with the human IP_3-3KA product complex (*26*) as the search model. Iterative rounds of manual model building in O (*32*) and coot (*33*) were followed by restrained refinement with TLS using Refmac5 (*34*), initially using tight NCS restraints between the two molecules in the asymmetric unit. Density modification was performed using ARP/wARP (*35*) to assist in the building of loop regions. Figures were prepared using pymol (www.pymol.org) and Genedoc (www.psc.edu/biomed/genedoc). The structure has been deposited in the Protein Data Bank as entry 2AQX.

RESULTS

Overall Structure. We have expressed, purified, and crystallized a construct of the C-terminal region of murine IP_3-3KB composed of both the catalytic and CaM binding domains. This protein has been demonstrated to retain both enzyme activity and Ca^{2+}-dependent responsiveness to CaM (Figure 2). The structure of mIP_3-3KB was determined in complex with ATP and Mg^{2+} to 2.5 Å resolution (crystallographic statistics are summarized in Table 1). The structure revealed two IP_3-3KB molecules in the crystallographic asymmetric unit, and these interact via an antiparallel β-sheet formed between residues in the CaM binding domain (Figure 3a). This strand will be called $\beta 0_N$ in accordance with the nomenclature of Gonzalez et al. which will be adopted for future discussion (*26*). Although there are numerous polar and nonpolar interactions between IP_3-3KB monomers in the crystal, the association is unusual for a biological dimer since the interchain interactions are mediated principally by the $\beta 0_N$ strands, and there is a separation between the globular folds of the respective catalytic domains (Figure 3). Analytical size exclusion chromatography of IP_3-3KB reveals that in the absence of CaM, IP_3-3KB is unequivocally monomeric (data not shown).

The overall structure of the IP_3-3KB catalytic domain is similar to that of the recently described isoform A, with an rmsd of 1.0 Å over an alignment of 231 Cα atoms (Figure 3b) (*26, 27*). IP_3-3K architecture is composed of highly homologous α/β N and C lobes and an all-α IP_3 binding

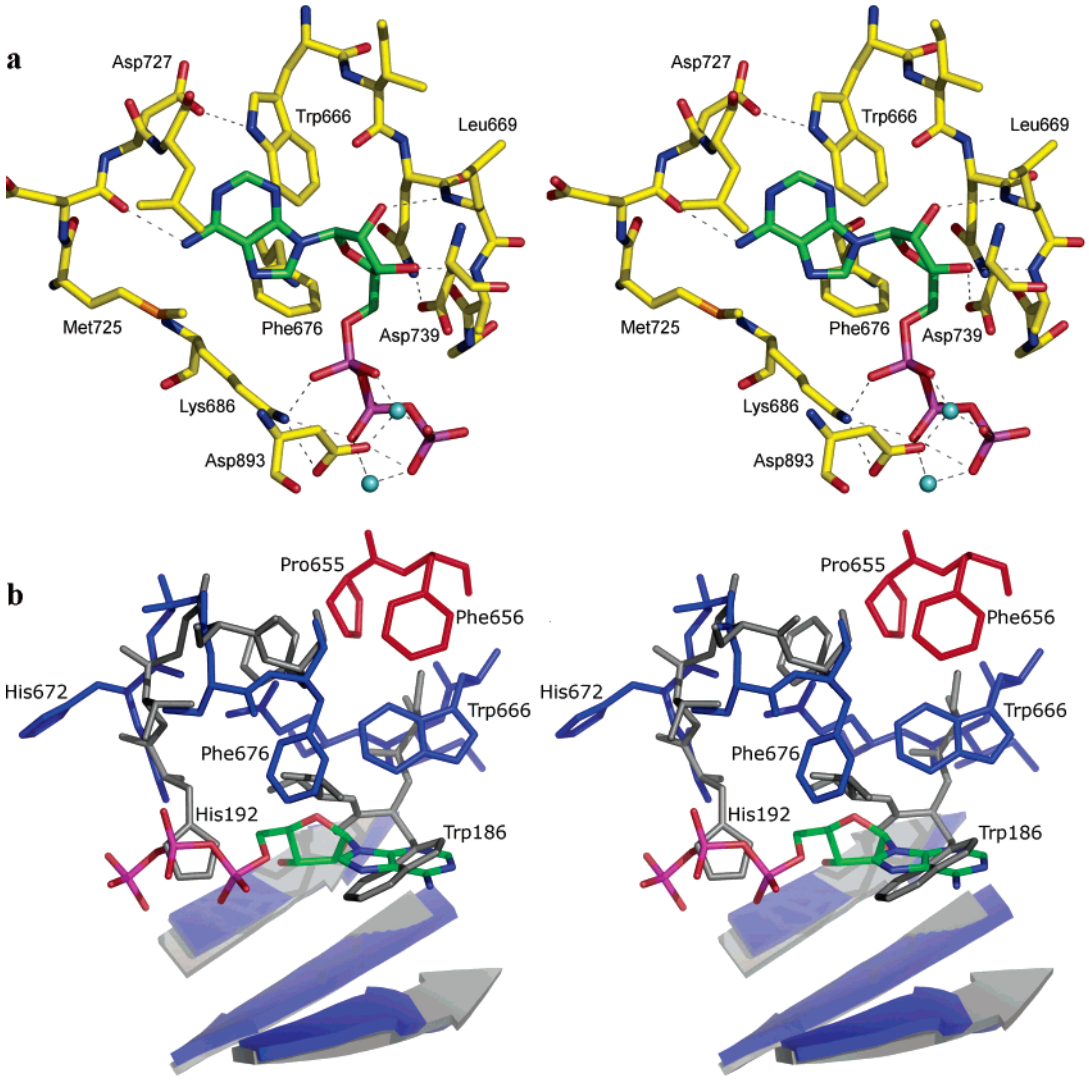

FIGURE 4: (a) Stereo diagram of ATP bound in the active site of IP_3-3KB. Atoms are colored according to element type, with green representing carbon in the ATP molecule and yellow representing carbon in the protein main chain. Polar bonds are represented by dashed lines. (b) Stereo diagram of a structural alignment between the apo IP_3-3KA structure (gray) and IP_3-3KB (chain A in blue, chain B in red, and ATP colored by element), showing the movement of Trp666 and His672 between the apo and ATP-bound forms of IP_3-3KA and IP_3-3KB, respectively.

lobe. The N and C lobes share a common topology with the protein kinases, with the IP_3 binding lobe inserted into the C lobe. The all-helical IP_3 binding lobe exhibits the highest average *B* factors of the IP_3-3KB structure, and a subset of helices ($\alpha 2_I$, $\alpha 3_I$, and $\alpha 4_I$) are rotated 18° away from the ATP binding site in IP_3-3KB relative to IP_3-3KA (Figure 3b). Comparison of IP_3-3KB and IP_3-3KA reveals that the IP_3 binding domain is hinged within the IP lobe at residue 757 at the C-terminus of helix $\alpha 1_I$, and residue 802 after helix $\alpha 4_I$ (Figure 3b). Helices $\alpha 2_I$ and $\alpha 4_I$ each contain residues which interact with bound IP_3 and IP_4, and binding interactions are also made with residues from both the N and C lobes (*26*). Since the N and C lobes overlap closely in the IP_3-3KB structure, the movement of the IP lobe consequently distorts the IP_3 binding site, precluding productive IP_3 binding in this crystal form (Figure 3b). This is consistent with the observation that addition of IP_3 to IP_3-3KB crystals results in rapid disintegration. The configuration of the IP_3 binding lobe might represent one stage in the catalytic or regulatory cycle, and a closing of the lobe may be initiated upon IP_3 binding. Clear density is visible for ATP in the IP_3-3KB structure (Figure 3c), presenting one further novel holo condition to the repertoire of ligand states currently described for the IP_3-3Ks. In addition, further ATP-binding residues are ordered in the IP_3-3KB structure, completing the description of the ATP binding site of IP_3-3K.

ATP Binding Site of IP_3-3KB. IP_3-3KB was crystallized in complex with ATP and two Mg^{2+} ions (Figure 4a). The ATP binding site is in a pocket between the N and C lobes, formed by β-sheets $\beta 1_N$ and $\beta 2_N$ above, and $\beta 1_C$ and $\beta 5_C$ below (Figure 3c). In the apo IP_3-3KA structure, the N-terminus of the structure starts at residue Ser185 (IP_3-3KB residue 665) which marks the start of helix $\alpha 0_N$ (Figures 1 and 3b) (*26*). Residues equivalent to the $\alpha 0_N$ helix are well ordered in the IP_3-3KB structure, allowing comparison of the conformation of this putative autoinhibitory helix in the ATP-bound form. The IP_3-3KB structure reveals that helix $\alpha 0_N$ of the apo IP_3-3KA structure is replaced by an extended loop conformation, which forms extensive contacts with the bound ATP (Figures 3c and 4a). This loop includes residues 666−671 which interact with the bound ATP molecule, with

hydrogen bonds from the main chain nitrogens of residues 669 and 670 to the ATP ribose 2′- and 3′-hydroxyls, respectively (Figure 4a). These hydrogen bonds replace and occlude the hydrogen bond described in IP_3-3KA between the terminal nitrogen of Lys334 (equivalent to IP_3-3KB residue 813) and the ribose 2′-hydroxyl group, although the polar interaction from the ribose 3′-hydroxyl to the side chain of Asp260 or Asp739 (IP_3-3KA or IP_3-3KB, respectively) is conserved in IP_3-3KB. The IP_3-3KB structure has revealed that the ATP substrate is almost fully enclosed due to the presence of this loop, and only the ATP β- and γ-phosphates are accessible to solvent (Figure 3c).

Importantly, the IP_3-3KB structure reveals the position adopted by the putative autoinhibitory residue Trp186 or Trp666 (IP_3-3KA or IP_3-3KB, respectively) in the ATP-bound IP_3-3K enzyme. In the structure of IP_3-3KB, the indole moiety of residue Trp666 forms part of the ATP binding site, forming hydrophobic interactions with the purine ring of the bound substrate. This is a shift in Cα position of 6.4 Å compared to the apo IP_3-3KA structure, as a consequence of the conformation rearrangement from helix to loop (Figure 4b). In addition to bonding with ATP, Trp666 exhibits hydrophobic interactions with the side chains of Phe676 and Ile684, and there is a polar interaction between the indole nitrogen and the carboxylic acid side chain of Asp727 (Figure 4a). As a possible consequence of the presence of Trp666, the ATP purine ring is rotated 15° relative to the substrate and product IP_3-3KA structures. The side chain of Trp666 also interacts with Pro655 and Phe656 from the second molecule in the crystallographic dimer (Figure 4b), revealing that intermolecular interactions may serve to stabilize the ATP binding site. The F656A mutant shows a reduced level of activation by Ca^{2+}/CaM, with an only 4-fold increase in activity compared to the 9-fold increase for the WT, indicating that this residue may contribute to CaM activation.

Mutagenesis of Trp666 results in an enzyme with ∼3-fold more ATPase activity than WT, under both basal and Ca^{2+}/CaM-activated conditions (Figure 2). This is consistent with a gating role for this residue in autoinhibition. However, it is clear that further residues are important for the structural mechanism of CaM activation, since the W666A enzyme retains a similar rank order activation by Ca^{2+}/CaM. In a manner similar to that of Trp666, His672 hydrogen bonds across the ATP binding site in the apo IP_3-3KA structure, occupying the position of the ATP β-phosphate (Figure 4b). H672A mutant IP_3-3KB has no detectable catalytic activity, despite the His672 side chain lying 5.6 Å from the bound ATP in the IP_3-3KB structure, and 5.4 Å from the modeled position of the IP_3.

CaM Binding Domain of IP_3-3KB. IP_3-3Ks exhibit a CaM recognition motif of the 1−10 class, characterized by two bulky, hydrophobic residues eight residues apart (residues Trp644 and Trp653 in IP_3-3KB; Figures 1 and 3b) (*36*, *37*). W644A mutant IP_3-3KB exhibits an undetectable level of activation by Ca^{2+}/CaM (Figure 2), although some activity is discernible after extended incubation times (data not shown). In contrast, the W653A enzyme appears to behave like WT under the conditions that were tested. Although some residues which are critical to CaM binding are disordered at the N-terminus of the IP_3-3KB structure (the structure becomes ordered at residue 650), IP_3-3KA residues 172−189 (IP_3-3KB residues 651−669) have also been shown to be critical in binding CaM (*20*). Equivalent residues are revealed to form a β-turn, β-sheet, and extended loop conformation in the IP_3-3KB structure while interacting with a second IP_3-3KB molecule.

IP_3-3KB CaM binding domain residues 651−654 form a type IV β-turn, with the side chain of Trp653 positioned in a cleft on the surface of the C lobe of the second molecule in the dimer, with intermolecular interactions between the side chains of Ile667 and Val819, with a hydrogen bond between the indole nitrogen and the main chain carbonyl oxygen of Gly817. A second intermolecular hydrogen bond from Trp653 occurs between the carbonyl oxygen and the main chain nitrogen of Gln668. Residue 668 is from the N lobe loop between $\beta 1_N$ and $\beta 0_N$, which exhibits extensive interactions with the bound ATP, as described in the preceding section and shown in Figure 4a. Further intermolecular interactions between CaM binding domain residues and the residues contacting the bound ATP occur as the side chains of Pro655 and Phe656 enclose the indole moiety of Trp666 from the corresponding IP_3-3KB molecule as it interacts with the ATP purine ring (Figure 4b). At residue 657, a β-conformation is assumed, and this extends to residue 665 forming an antiparallel β-sheet ($\beta 0_N$) with the same strand in the corresponding molecule (Figure 3a, and colored in Figure 1).

DISCUSSION

The IP_3-3KB structure has provided the atomic structure of the catalytic and CaM domains of a protein critical to the development of the immune system. This structure has also completed the structural description of the IPK catalytic domain, and provided the first structure of the CaM binding domain. CaM binding motifs typically form amphipathic α-helices, although they can be unstructured in solution prior to binding of CaM (*37*). In this manner, a helix may form upon CaM binding from the disordered residues at the N-terminus of IP_3-3KB. There is evidence that some peptides do not bind to CaM as α-helices, but instead assume an extended conformation (*38*). Noncanonical CaM binding was also revealed in the structure of the complex between CaM and the CaM binding peptide from CaMKK, which included a hairpinlike conformation in the bound substrate (*39*).

Although most reports on the multimeric state of IP_3-3Ks indicate that these enzymes exist as monomers in solution (*26*, *40*), size-exclusion experiments have shown that upon addition of CaM, IP_3-3K purified from rat brain undergoes a greater shift in mobility than would be expected from the formation of a 1:1 IP_3-3K−CaM complex, leading to the conclusion that IPKs may dimerize upon addition of CaM (*41*). The intermolecular interactions revealed in the IP_3-3KB crystal may represent a transient biological interaction, stabilized by the crystal lattice, which may occur under particular conditions, or as a consequence of ligand binding. It is also possible that the β-sheet observed in the IP_3-3KB structure may have been induced by the proximity of the IP_3-3KB molecules in the crystal lattice, and that the $\beta 0_N$ strand is either disordered or in an alternative conformation in solution. A further possibility is that the antiparallel sheet observed is mimicking biological interactions made with a nonidentical molecule.

Extensive buried surfaces were noted in both published descriptions of IP_3-3KA crystal structures, with the IP_3-3KA

crystallographic dimer interaction mediated via the $\beta 3_C$ strands. It is worth noting that the two published IP_3-3KA structures exhibit a common crystal lattice, and both groups provide evidence that the observed dimer does not exist in solution under the conditions that were studied (in the absence of Ca^{2+}/CaM). The IP_3-3KA crystal interaction is not conserved in the IP_3-3KB crystal. Clearly, further study will be required to determine the biological role of the dimers observed in the IP_3-3K crystal structures.

The IP_3-3KB CaM domain residues are linked through the protein backbone to residues forming part of the ATP binding site, revealing an environment more enclosed and hydrophobic than that previously described for IP_3-3KA. Among IP_3-3KA residues which occupied the ATP binding site to the exclusion of ATP in the apo structure, Trp666 and His672 have been shown to swing out of the active site in a conformation rearrangement from helix to loop. Furthermore, Trp666 has been shown to form part of the ATP binding site, contributing hydrophobic interactions with the ATP purine ring. The 4−5-fold increase in activity for both basal and CaM-activated W666A mutant IP_3-3KB suggests that Trp666 may be acting to achieve a reduced level of basal activity prior to cytoplasmic Ca^{2+} influx and CaM binding. Since the IP_3-3KB structure has revealed apparently favorable interactions between Trp666 and the bound ATP, it appears likely that Trp666 reduces enzyme turnover by reducing the on-rate of ATP binding by stabilizing the apo conformation.

Mutagenesis of the equivalent tryptophan residue in IP_3-3KA resulted in a 40% drop in activity compared to that of WT (*26*), which appears to contradict the IP_3-3KB results. However, the difference may be explained by the difference in experimental conditions since ATP is highly limiting in our assay. This would be expected to accentuate the proposed gating effect of the $\alpha 0_N$ helix if it acts in a manner competitive with ATP, as would be predicted from the structure. In saturating quantities of ATP, the effect of competitive autoinhibition mediated by Trp666 should be minimized, and under these circumstances, it is possible that a reduction in V_{max} may occur in the Trp → Ala mutant as a consequence of the lost binding interactions provided by the indole group in the ATP-bound IP_3-3KB structure.

Curiously, His672 is revealed to be crucial to enzyme activity, despite the imidazole side chain lying >5 Å from the position of either substrate. Certainly, His672 is capable of rearranging to more closely approach the active site, since in the apo IP_3-3KA structure this residue is found hydrogen bonding across the ATP site to the catalytic Asp414 (IP_3-3KB residue 893). Bonding across the empty ATP binding site would be suggestive of a gating role for this residue, which was disordered in the holo IP_3-3KA structures. However, the loss of activity in the H672A mutant is indicative of a more central role in catalysis. This may occur during an uncharacterized conformation in the catalytic cycle, or may be occurring through an unknown mechanism. For example, it is possible that in the apo IP_3-3KA structure, this side chain may be acting to chaperone the catalytic aspartate prior to ATP binding.

The definition of new residues enclosing the bound ATP indicates that access to the ATP binding site may be limited to an entry point near the position of the bound γ-phosphate. Under these circumstances, binding of IP_3 or IP_4 on the opposing face of the IP lobe may present a steric barrier to nucleotide exchange. Such an arrangement would require an ordered reaction mechanism where ATP docks to the enzyme first, which offers an explanation for the substrate and product enzyme inhibition by IP_3 or IP_4 observed in the IP_3-3Ks (*42*).

CONCLUSIONS

In this work, we have described the structure of murine IP_3-3KB, an enzyme vital to the development of the immune system. This structure has completed the description of the ATP binding site of IP_3-3K. Structural comparison has revealed a conformational rearrangement in the ATP site from a helical conformation in apo IP_3-3KA to a loop conformation in IP_3-3KB. In IP_3-3KA, this helix occupies the ATP site in a manner that would preclude ATP binding, while in IP_3-3KB, the same residues form part of the ATP binding site and appear to interact favorably with the bound substrate. The IP_3-3KB structure has also revealed that the residues involved in this conformational rearrangement are linked to a β-sheet composed of residues from the CaM binding domain, and this conformational shift could represent a structural mechanism of CaM activation for the IP_3-3Ks.

ACKNOWLEDGMENT

Thanks to Ben Wen, Yina Huang, and Al Parker for materials and useful discussions and to Robin Irvine for comments on the manuscript. Thanks to Peter Schultz for continued support. The work in this paper is based on experiments conducted at beamlines 5.0.3 and 5.0.2 of the ALS. The ALS is supported by the Director, Office of Science, Office of Basic Energy Sciences, Material Sciences Division of the U.S. Department of Energy, under Contract DE-AC03-76SF00098 at Lawrence Berkeley National Laboratory. We thank all of the staff of these beamlines for their continued support.

REFERENCES

1. Irvine, R. F., and Schell, M. J. (2001) Back in the water: The return of the inositol phosphates, *Nat. Rev. Mol. Cell Biol. 2*, 327−38.
2. Irvine, R. (2001) Inositol phosphates: Does IP_4 run a protection racket? *Curr. Biol. 11*, R172−4.
3. Wen, B. G., Pletcher, M. T., Warashina, M., Choe, S. H., Ziaee, N., Wiltshire, T., Sauer, K., and Cooke, M. P. (2004) Inositol 1,4,5-trisphosphate 3 kinase B controls positive selection of T cells and modulates Erk activity, *Proc. Natl. Acad. Sci. U.S.A. 101*, 5604−9.
4. Wen, B. G., Miller, A. T., Huang, Y. H., Pletcher, M. T., Warashina, M., Choe, S. H., Ziaee, N., Wiltshire, T., Cooke, M. P., and Sauer, K. (2004) *Ms. T-less*, an ENU-Induced Mouse Mutant Linking Impaired Expression of Ins(1,4,5)P3 3-kinase B (Itpkb) to Defective Erk Activation and Blocked Positive Selection, *Immunology 2004*, pp 85−90, Medimont S.r.l., Bologna, Italy.
5. Cullen, P. J., Hsuan, J. J., Truong, O., Letcher, A. J., Jackson, T. R., Dawson, A. P., and Irvine, R. F. (1995) Identification of a specific Ins(1,3,4,5)P4-binding protein as a member of the GAP1 family, *Nature 376*, 527−30.
6. Pattni, K., and Banting, G. (2004) Ins(1,4,5)P3 metabolism and the family of IP3-3 Kinases, *Cell Signalling 16*, 643−54.
7. Takazawa, K., Perret, J., Dumont, J. E., and Erneux, C. (1991) Molecular cloning and expression of a new putative inositol 1,4,5-trisphosphate 3-kinase isoenzyme, *Biochem. J. 278* (Part 3), 883−6.
8. Choi, K. Y., Kim, H. K., Lee, S. Y., Moon, K. H., Sim, S. S., Kim, J. W., Chung, H. K., and Rhee, S. G. (1990) Molecular

cloning and expression of a complementary DNA for inositol 1,4,5-trisphosphate 3-kinase, *Science 248*, 64−6.
9. Dewaste, V., Pouillon, V., Moreau, C., Shears, S., Takazawa, K., and Erneux, C. (2000) Cloning and expression of a cDNA encoding human inositol 1,4,5-trisphosphate 3-kinase C, *Biochem. J. 352* (Part 2), 343−51.
10. Jun, K., Choi, G., Yang, S. G., Choi, K. Y., Kim, H., Chan, G. C., Storm, D. R., Albert, C., Mayr, G. W., Lee, C. J., and Shin, H. S. (1998) Enhanced hippocampal CA1 LTP but normal spatial learning in inositol 1,4,5-trisphosphate 3-kinase(A)-deficient mice, *Learn. Mem. 5*, 317−30.
11. Mailleux, P., Takazawa, K., Erneux, C., and Vanderhaeghen, J. J. (1991) Inositol 1,4,5-trisphosphate 3-kinase distribution in the rat brain. High levels in the hippocampal CA1 pyramidal and cerebellar Purkinje cells suggest its involvement in some memory processes, *Brain Res. 539*, 203−10.
12. Nalaskowski, M. M., Bertsch, U., Fanick, W., Stockebrand, M. C., Schmale, H., and Mayr, G. W. (2003) Rat inositol 1,4,5-trisphosphate 3-kinase C is enzymatically specialized for basal cellular inositol trisphosphate phosphorylation and shuttles actively between nucleus and cytoplasm, *J. Biol. Chem. 278*, 19765−76.
13. Vanweyenberg, V., Communi, D., D'Santos, C. S., and Erneux, C. (1995) Tissue- and cell-specific expression of Ins(1,4,5)P3 3-kinase isoenzymes, *Biochem. J. 306* (Part 2), 429−35.
14. Soriano, S., Thomas, S., High, S., Griffiths, G., D'Santos, C., Cullen, P., and Banting, G. (1997) Membrane association, localization and topology of rat inositol 1,4,5-trisphosphate 3-kinase B: Implications for membrane traffic and Ca^{2+} homoeostasis, *Biochem. J. 324* (Part 2), 579−89.
15. Dewaste, V., Moreau, C., De Smedt, F., Bex, F., De Smedt, H., Wuytack, F., Missiaen, L., and Erneux, C. (2003) The three isoenzymes of human inositol-1,4,5-trisphosphate 3-kinase show specific intracellular localization but comparable Ca^{2+} responses on transfection in COS-7 cells, *Biochem. J. 374*, 41−9.
16. Pouillon, V., Hascakova-Bartova, R., Pajak, B., Adam, E., Bex, F., Dewaste, V., Van Lint, C., Leo, O., Erneux, C., and Schurmans, S. (2003) Inositol 1,3,4,5-tetrakisphosphate is essential for T lymphocyte development, *Nat. Immunol. 4*, 1136−43.
17. Dewaste, V., Roymans, D., Moreau, C., and Erneux, C. (2002) Cloning and expression of a full-length cDNA encoding human inositol 1,4,5-trisphosphate 3-kinase B, *Biochem. Biophys. Res. Commun. 291*, 400−5.
18. Pattni, K., Millard, T. H., and Banting, G. (2003) Calpain cleavage of the B isoform of Ins(1,4,5)P3 3-kinase separates the catalytic domain from the membrane anchoring domain, *Biochem. J. 375*, 643−51.
19. Woodring, P. J., and Garrison, J. C. (1997) Expression, purification, and regulation of two isoforms of the inositol 1,4,5-trisphosphate 3-kinase, *J. Biol. Chem. 272*, 30447−54.
20. Takazawa, K., and Erneux, C. (1991) Identification of residues essential for catalysis and binding of calmodulin in rat brain inositol 1,4,5-trisphosphate 3-kinase, *Biochem. J. 280* (Part 1), 125−9.
21. Erneux, C., Moreau, C., Vandermeers, A., and Takazawa, K. (1993) Interaction of calmodulin with a putative calmodulin-binding domain of inositol 1,4,5-triphosphate 3-kinase. Effects of synthetic peptides and site-directed mutagenesis of Trp165, *Eur. J. Biochem. 214*, 497−501.
22. Sim, S. S., Kim, J. W., and Rhee, S. G. (1990) Regulation of D-myo-inositol 1,4,5-trisphosphate 3-kinase by cAMP-dependent protein kinase and protein kinase C, *J. Biol. Chem. 265*, 10367−72.
23. Communi, D., Vanweyenberg, V., and Erneux, C. (1997) D-myo-inositol 1,4,5-trisphosphate 3-kinase A is activated by receptor activation through a calcium:calmodulin-dependent protein kinase II phosphorylation mechanism, *EMBO J. 16*, 1943−52.
24. Rogers, S., Wells, R., and Rechsteiner, M. (1986) Amino acid sequences common to rapidly degraded proteins: The PEST hypothesis, *Science 234*, 364−8.
25. Molinari, M., Anagli, J., and Carafoli, E. (1995) Purification of μ-calpain by a novel affinity chromatography approach. New insights into the mechanism of the interaction of the protease with targets, *J. Biol. Chem. 270*, 2032−5.
26. Gonzalez, B., Schell, M. J., Letcher, A. J., Veprintsev, D. B., Irvine, R. F., and Williams, R. L. (2004) Structure of a human inositol 1,4,5-trisphosphate 3-kinase: Substrate binding reveals why it is not a phosphoinositide 3-kinase, *Mol. Cell 15*, 689−701.
27. Miller, G. J., and Hurley, J. H. (2004) Crystal structure of the catalytic core of inositol 1,4,5-trisphosphate 3-kinase, *Mol. Cell 15*, 703−11.
28. Soderling, T. R., and Stull, J. T. (2001) Structure and regulation of calcium/calmodulin-dependent protein kinases, *Chem. Rev. 101*, 2341−52.
29. Otwinowski, Z., and Minor, W. (1997) Processing of X-ray Diffraction Data Collected in Oscillation Mode, *Methods Enzymol. 276*, 307−26.
30. Collaborative Computational Project, No. 4 (1994) The CCP4 suite: Programs for protein crystallography, version 3.1, *Acta Crystallogr. D50*, 760−3.
31. Stroroni, L. C., McCoy, A. J., and Read, R. J. (2004) Likelihood enhanced fast rotation functions, *Acta Crystallogr. D60*, 432−8.
32. Jones, T. A., Zou, J. Y., Cowan, S. W., and Kjeldgaard, M. (1991) Improved methods for building protein models in electron density maps and the location of errors in these models, *Acta Crystallogr. A47*, 110−9.
33. Emsley, P., and Cowtan, K. (2004) Coot: Model-building tools for molecular graphics, *Acta Crystallogr. D60*, 2126−32.
34. Murshudov, G. N., Vagin, A. A., and Dodson, E. J. (1997) Refinement of macromolecular structures by the maximum-likelihood method, *Acta Crystallogr. D53*, 240−55.
35. Perrakis, A., Harkiolaki, M., Wilson, K. S., and Lamzin, V. S. (2001) ARP/wARP and molecular replacement, *Acta Crystallogr. D57*, 1445−50.
36. Yap, K. L., Kim, J., Truong, K., Sherman, M., Yuan, T., and Ikura, M. (2000) Calmodulin target database, *J. Struct. Funct. Genomics 1*, 8−14.
37. Rhoads, A. R., and Friedberg, F. (1997) Sequence motifs for calmodulin recognition, *FASEB J. 11*, 331−40.
38. Porumb, T., Crivici, A., Blackshear, P. J., and Ikura, M. (1997) Calcium binding and conformational properties of calmodulin complexed with peptides derived from myristoylated alanine-rich C kinase substrate (MARCKS) and MARCKS-related protein (MRP), *Eur. Biophys. J. 25*, 239−47.
39. Osawa, M., Tokumitsu, H., Swindells, M. B., Kurihara, H., Orita, M., Shibanuma, T., Furuya, T., and Ikura, M. (1999) A novel target recognition revealed by calmodulin in complex with Ca^{2+}-calmodulin-dependent kinase kinase, *Nat. Struct. Biol. 6*, 819−24.
40. Takazawa, K., Passareiro, H., Dumont, J. E., and Erneux, C. (1989) Purification of bovine brain inositol 1,4,5-trisphosphate 3-kinase. Identification of the enzyme by sodium dodecyl sulphate/polyacrylamide-gel electrophoresis, *Biochem. J. 261*, 483−8.
41. Johanson, R. A., Hansen, C. A., and Williamson, J. R. (1988) Purification of D-myo-inositol 1,4,5-trisphosphate 3-kinase from rat brain, *J. Biol. Chem. 263*, 7465−71.
42. Nalaskowski, M. M., and Mayr, G. W. (2004) The families of kinases removing the Ca^{2+} releasing second messenger Ins(1,4,5)-P3, *Curr. Mol. Med. 4*, 277−90.

BI051256Q